

Onset of criticality in hyper-auxetic polymer networks

Andrea Ninarello,^{*} José Ruiz-Franco,^{*} and Emanuela Zaccarelli[†]

CNR Institute of Complex Systems, Uos Sapienza, Piazzale Aldo Moro 2, 00185, Roma, Italy and

Department of Physics, Sapienza University of Rome, Piazzale Aldo Moro 2, 00185 Roma, Italy

(Dated: August 13, 2021)

Against common sense, auxetic materials expand when stretched or contract when compressed by uniaxial strain, being characterized by a negative Poisson's ratio ν . The amount of perpendicular deformation in response to the applied force can be at most equal to the imposed one, so that $\nu = -1$ is the lowest bound for the mechanical stability of solids, a condition here defined as “hyper-auxeticity”. In this work, we numerically show that ultra-low-crosslinked polymer networks under tension display hyper-auxetic behavior at a finite crosslinker concentration. At this point, the nearby mechanical instability triggers the onset of a critical-like transition between two states of different densities. This phenomenon displays similar features as well as important differences with respect to gas-liquid phase separation. Since our model is able to faithfully describe real-world hydrogels, the present results can be readily tested in laboratory experiments, paving the way to explore this unconventional phase behavior.

The mechanical response of a material subjected to uniaxial strain in the direction orthogonal to the deformation is quantified via the Poisson's ratio ν , defined as the negative ratio between transverse and longitudinal deformation. For the most common three-dimensional materials ν is positive, so that these expand (contract) in response to a compressive (extensional) strain. This situation is schematically illustrated in Fig. 1(a). On the contrary, auxetic materials are characterized by negative values of ν , meaning that they become thicker perpendicularly to the deformation axis, as shown in Fig. 1(b). Auxetic behaviour has been so far reported in a large variety of systems, including foams, polymers, fibers, tendons and crystals [1–7]. Recently, a strong research interest has been devoted towards auxetic metamaterials in which the elastic properties can be tailored by geometrical design [8–10] or by pruning methods [11]. Besides geometrical reasons, a negative ν can also be obtained by exploiting critical behavior and phase transitions, as in the case of ferroelastic materials in the vicinity of the Curie point [12, 13].

Within linear elasticity theory [14], the appearance of a negative ν can be related to a decrease of the bulk modulus K with respect to the shear modulus G , namely to an isotropic softening of the material. A vanishing K echoes the divergence of the isothermal compressibility occurring at a gas-liquid critical point. However, the presence of a finite shear modulus, as found in polymer networks such as hydrogels, may induce a negative ν . Pioneering evidence of a negative Poisson's ratio has been reported for these systems close to the so-called volume phase transition [15–17]: in this case, a variation in temperature changes the affinity of the polymer to the solvent, favouring monomer-monomer aggregation, in full analogy with the gas-liquid critical point, but with the additional constraint of infinite connectivity. Another thermodynamic parameter that influences the network properties without affecting monomeric interactions is pressure, or tension. Indeed, theoretical works have addressed the occurrence of auxeticity in two-dimensional models of networks under tension [18, 19].

It is important to notice that these studies have flourished about twenty years ago, but the interest in hydrogel and microgel networks has increased again in the last few years, thanks to advances in chemical and *in silico* synthesis. In particular, it became recently possible to tune the amount of branching points (crosslinkers) to yield *ultra-low-crosslinked* networks [20–23]. In parallel, numerical efforts have been able to realize fully-connected, disordered networks with arbitrary density and crosslinker concentrations [24, 25].

In this article, we numerically investigate the elastic properties of polymer networks under tension and demonstrate that auxeticity naturally emerges in the ultra-low-crosslinked limit. Combining stress-strain and equilibrium simulations, we show that low-density polymeric networks exhibit a non-monotonic behavior of K as well as ν , the latter becoming increasingly negative with reducing crosslinker concentration c . This phenomenology is found for both ordered diamond-like and disordered hydrogel realizations, indicating that there is no need of a specific topology to observe auxeticity in polymer networks. Remarkably, we do not find that this behavior continuously evolves down to $c \rightarrow 0$. Rather, it hits a mechanical *critical* point, that we name *hyper-auxetic* point, at a finite $c = c^* \sim 0.35\%$ where $\nu = -1$. Owing to the fact that the moduli would become negative, this value denotes the lowest limit of mechanical stability, even though this condition is not yet fully understood [7, 26, 27]. At this point, we detect the onset of a coexistence between two different states: a low density and a high density one. These results call for an analogy with the well-known gas-liquid phase transition in attractive fluids, but with two important differences: (i)

^{*} These authors contributed equally

[†] Corresponding author: emanuela.zaccarelli@cnr.it

the lack of attraction between the monomers due to the good solvent conditions of the polymer networks and (ii) the presence of critical-like density fluctuations which do not seem to obey Ising-like statistics within the present numerical resolution.

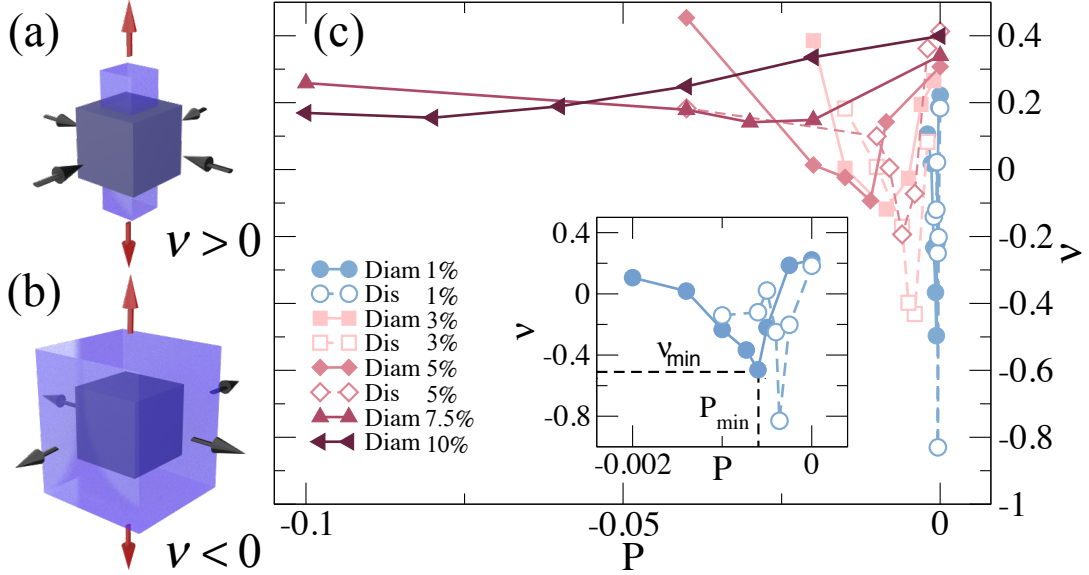


Figure 1. **Auxetic behavior of ordered and disordered hydrogels.** Illustration of (a) standard ($\nu > 0$) versus (b) auxetic ($\nu < 0$) behavior; (c) calculated Poisson's ratio ν as a function of negative pressure P for different values of crosslinker concentration $c = 1, 3, 5, 7.5\%$ both for ordered (Diam, full symbols) and disordered (Dis, empty symbols) networks. Inset: zoom of $c = 1\%$, where the minimum values of pressure and Poisson's ratio, P_{min} and ν_{min} respectively, are indicated for the Diam-1% case.

We start by calculating the elastic properties of diamond networks (Diam) for different values of the crosslinker concentration c for negative pressures starting from $P = 0$. For each state point, we independently evaluate three moduli: while the bulk modulus K is obtained from equilibrium NPT runs, the Young modulus Y and the Poisson's ratio ν are estimated from strain-stress simulations, as described in the Methods section. We report ν in Fig. 1(c) for hydrogels with different c , while the corresponding K and Y are shown in Fig. S1 of the SI. All moduli display a similar behavior: they initially decrease, then reach a minimum at intermediate values of pressures, and finally increase again for very negative P . The minima become more and more pronounced for lower and lower c , remaining visible at all c for ν and K , while disappearing for Y when $c \gtrsim 3\%$. Remarkably, we find that the different networks display a positive value of ν both for $P = 0$ and for very large negative pressures, while auxetic behavior is observed for $c \lesssim 5\%$ in a finite range of tensions, that become smaller and closer to zero pressure as c decreases. We denote the minimum value reached by ν as ν_{min} and its corresponding pressure as P_{min} (see inset of Fig. 1).

So far we exclusively discussed ordered networks. However, in real world realizations, hydrogels are intrinsically disordered and frequently made of chains whose length is exponentially distributed [28, 29]. Being able to prepare hydrogels with these features, as described in Methods, we find that disordered networks (Dis) show the same phenomenology as ordered ones when subjected to tensions, with auxeticity also emerging for $c \lesssim 5\%$ (see Fig. 1). Interestingly, we observe lower values of ν_{min} for disordered hydrogels with respect to ordered ones at the same crosslinker concentration, as shown in the inset of Fig. 1. In particular, we find $\nu_{min} \approx -0.8$ for the Dis-1% network. We ascribe this effect to the larger heterogeneity characterizing disordered systems, independently of the specific network topology. Indeed, the same qualitative phenomenology is observed for all examined realizations (see Fig. S2). Since the preparation procedure is based on the self-assembly of patchy particles [24, 25], we cannot easily obtain disordered networks with smaller values of c , due to the nearby occurrence of phase separation. Thus, for lower degree of crosslinking, we focus only on diamond networks, having shown in Fig. 1 that there is no major qualitative effect of the underlying topology on auxeticity, in line with previous results for ordered or partially ordered topologies [8–11].

By further decreasing c for Diam-N we still observe a progressive decrease of ν_{min} . To have a better understanding of the mechanical behaviour of the system, we report in Fig. 2(a) the longitudinal vs the negative transverse strain for $c = 0.35\%$ at different values of pressure. We clearly see that, for $P = 0$, the slope, that is precisely our numerical estimate of ν , is positive. Then, by progressively reducing P , ν becomes negative, down to $\nu_{min} \simeq -1$ within numerical uncertainty. At this point, the system has reached the limit of mechanical stability, so that state points with $\nu < -1$ are not allowed. We therefore consider $c^* \simeq 0.35\%$ as the critical fraction of crosslinker at which a mechanical critical

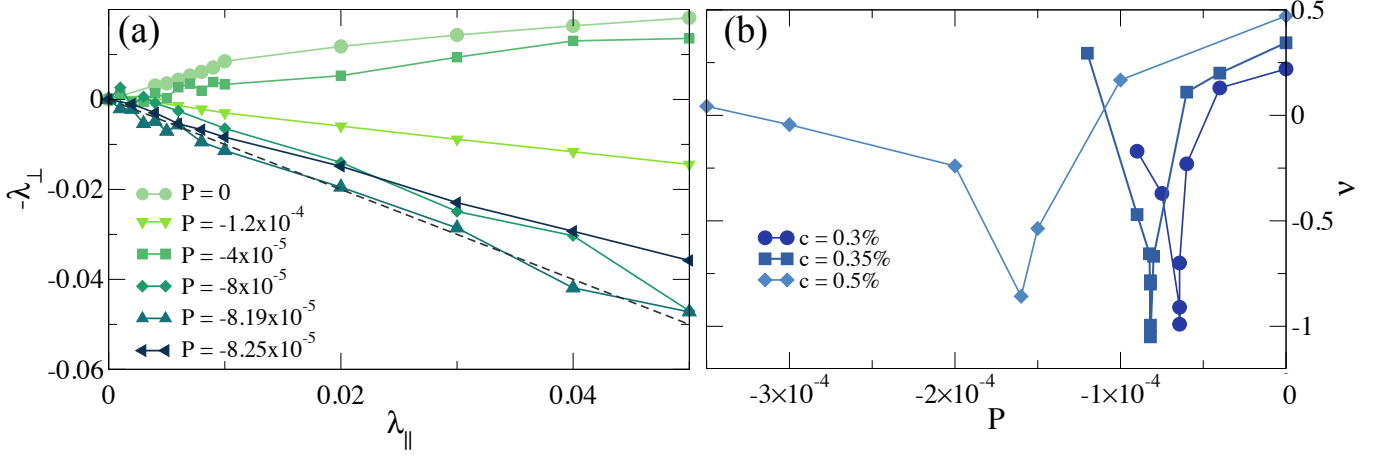


Figure 2. **Emergence of hyper-auxetic behavior and mechanical instability.** (a) Negative transverse strain (λ_{\perp}) as a function of longitudinal strain (λ_{\parallel}) for $c = 0.35\%$ system for different values of pressure. The dashed straight line has negative unitary coefficient well-approximating the data for $P = P_{min} = -8.19 \times 10^{-5}$ (hyper-auxetic point); (b) Poisson's ratio ν as a function of negative P for ultra-low-crosslinked diamond hydrogels with $c = 0.30\%, 0.35\%, 0.5\%$.

point is encountered and define state points with $\nu = -1$ as hyper-auxetic. Interestingly, we find that, upon further increasing tension, the slope starts to increase again, as shown in Fig. 2(a). The behaviour of ν vs P is reported for three ultra-low values of c respectively above, at and below c^* in Fig. 2(b). These findings indicate that the system reaches a hyper-auxetic condition also for $c < c^*$. This phenomenology thus occurs for ultra-low-crosslinked networks in general, with the system reaching $\nu_{min} = -1$ at a small, finite negative pressure.

This behavior is very reminiscent of what happens close to a thermodynamic second-order phase transition, such as the gas-liquid one, where a homogeneous system becomes thermodynamically unstable due to the divergence of the isothermal compressibility. To avoid this, the system thus separates into two phases characterized by a different density. It is now interesting to investigate by which mechanism ultra-low-crosslinked hydrogels deal with the presence of the mechanical instability and which similarities or differences with respect to the gas-liquid scenario occur. To this aim, we report the behavior of the Diam - 0.35% density fluctuations with respect to time in Fig. S4 for different values of pressure, detecting the onset of critical-like fluctuations. In particular, we focus in Fig. 3(a) on the state point closest to the mechanical instability, for which it is evident that the system fluctuates between two states, an expanded and a compressed one, respectively illustrated in the corresponding snapshots of Fig. 3(b,c). We note that the elastic moduli of the two states are also quite different and, indeed, we calculate them separately, as shown in Fig S3. We find that both phases have a Poisson's ratio rather close to -1 within statistical uncertainty. Thus, the mechanism of density jump is the one allowing the system to avoid the mechanical instability, in full analogy with gas-liquid phase separation. This is also confirmed by looking at the behavior of the (negative) pressure against density shown in Fig. 3(d). We note that, for the present study, the crosslinker concentration plays the role of temperature in phase-separating fluids: as c becomes smaller, P becomes progressively flatter and a critical-like point is observed for these putative equation of states, which depend on a geometric rather than a thermodynamic control variable. For $c \leq c^*$, a clear discontinuity in density is observed, signaling a first-order-like transition between the two states.

To get better microscopic insights of this behaviour, we report the average bond length l_{bond} as a function of P in Fig. 3(e). From a geometrical perspective, lowering the pressure towards more negative values has the effect of stretching the chains, as demonstrated by the growth of l_{bond} . However, it is important to note that this behavior arises only when $P \approx P_{min}$, i.e. when ν starts to increase again beyond its minimum value. Since it is well-known that entropy plays a fundamental role for phase behaviour of polymer systems [30], we also quantify the effect of entropy by calculating the average single-chain entropy s_l within a Langevin-approximation (see Methods and Ref. [25]). Relying on this controlled approximation, we detect a decrease of s_l by roughly one order of magnitude going from the compressed to the expanded state, as shown in Figs. 3(f) and S6. At the same time, monitoring the average total energy (see Fig. S5), we find no remarkable change, confirming the entropic origin of the transition.

Finally, aiming to build a correspondence with thermodynamic phase separation, we calculate the order parameter M , equivalent to the one used to describe the gas-liquid transition, that is composed by density and energy fluctuations via a mixing parameter [31]. Since we find that for the present system the total potential energy is not correlated with density, differently from one-component fluids [32], we restrict the calculation to the energy of non-bonded monomers, which is instead found to be correlated with density (see Fig. S5). Starting from very asymmetric distributions for

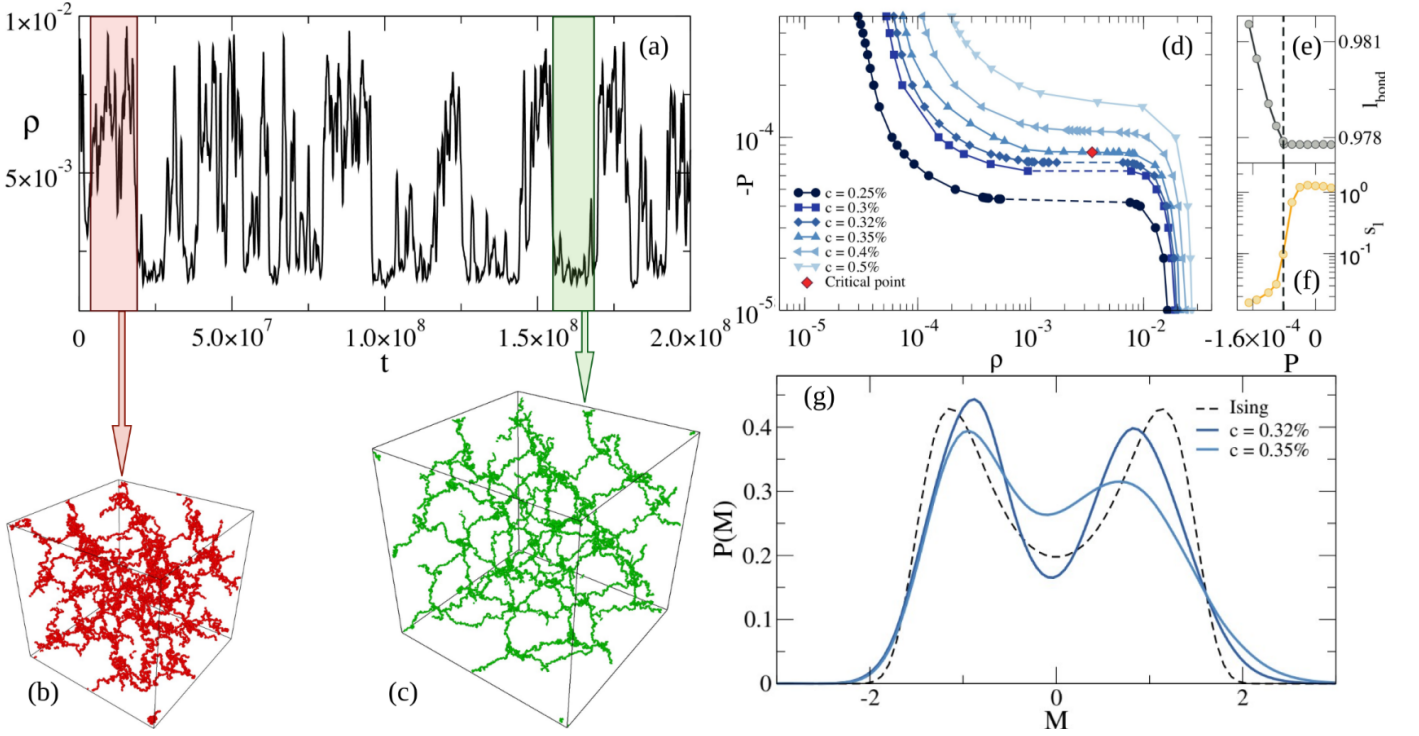


Figure 3. **Critical nature of the transition.** (a) Density fluctuations as a function of time for the Diam - 0.35% network at $P = -8.19 \times 10^{-5}$; simulation snapshots of the compressed (b) and expanded states (c) among which the system fluctuates; (d) “equation of state” of the diamond networks showing P as a function of ρ for different values of c . The red diamond symbol indicates the approximate location of the onset of mechanical instability and critical-like behavior. To improve visualization, data are shown using the opposite sign for pressure on a log-log scale; average values of (e) bond length l_{bond} and (f) single-chain entropy s_l as a function of P for the Diam - 0.35% network. The dashed line indicates the hyper-auxetic point ($P_{min} = -8.19 \times 10^{-5}$); (g) probability distribution of the order parameter $M = \rho + s e_{nb}$, where s is the mixing parameter and e_{nb} is the non-bonded particles potential energy, for Diam - 0.32% and 0.35% networks. The curves are reported for $P = -6.8898 \times 10^{-5}$, $s = 2.59$ and $P = -8.9135 \times 10^{-5}$, $s = 1.25$, respectively, representing distributions that are found to be closest with respect to the Ising one through single histogram reweighting.

the density only (see Fig. S7), we calculate the probability distribution of the order parameter $P(M)$. Through the histogram reweighting technique, we finally estimate the one that minimizes the mean-square error with respect to the expected 3D Ising universal distribution, which is shown in Fig. 3(g) for two state points close to the mechanical instability at two different values of c . The resulting $P(M)$ ’s for ultra-low-crosslinked hydrogels are characterized by a slightly asymmetric shape, not perfectly centered in zero with rather broad peaks. We find a qualitative disagreement with the Ising behaviour that might be due to an intrinsic difference of the network system with respect to associating molecules or to insufficient sampling. In the first case, we may speculate that the infinite connectivity of the network may bias the way in which the density fluctuates as compared to unbound particles. Alternatively, the deviation may be attributed to the fact that, in the present simulations, c cannot be varied in a continuous way, as normally done with temperature close to the gas-liquid critical point, thus hindering a detailed exploration of the critical properties of the current transition. However, we note that we found deviations from the Ising expectations for all examined c values, moving either below or above c^* , finding no systematic improvement. Future work will be needed to properly address this issue.

The present results, obtained by means of extensive simulations to calculate the elastic properties of ultra-low crosslinked polymer networks at negative pressures, report the emergence of auxetic behavior for $c \lesssim 5\%$ independently of the specific geometry of the network. It is important to note that, if we limited our results to not-too-small values of c , we would have legitimately expected a continuous behavior of the system until approaching the limit of stability ($\nu = -1$) at $P = 0$. This was also suggested by the dependence of P_{min} and ν_{min} with respect to c , that is reported in Fig. S8: while ν_{min} decreases logarithmically, P_{min} is found to obey a quadratic power-law behavior in c for all examined networks and spanning a range of more than three decades. Hence, our initial conjecture was that the system would smoothly transform, upon decreasing the number of crosslinkers, from a low-density, low-connectivity network into a system of polymer chains at $P = 0$, the latter being a stable system in good solvent conditions as the

present ones but with a shear elastic modulus that is equal to zero. Surprisingly, instead of this scenario, we found the occurrence of hyper-auxetic behavior ($\nu = -1$) at a finite crosslinker concentration, $c^* \simeq 0.35\%$, even for a regular geometry such as the diamond one. Since below this value the network becomes mechanically unstable, a transition between two states, a compressed and an expanded state, is thus encountered at this critical low crosslinking ratio, also accompanied by large density fluctuations reminiscent of critical ones in gas-liquid phase separation, shown in Figs. 3(a) and S4.

It is important to note that these observations pertain to ultra-low-crosslinked networks, that are nowadays within experimental reach [20, 33, 34]. While experimental realizations are necessarily disordered, our numerical predictions suggest that disordered networks should display a slightly larger value of c^* , not too far from 1% (see Fig. 1), with respect to the diamond case, which would actually favour the experimental observation of this mechanical critical point and a thorough exploration of its vicinity both from above and from below c^* . Notably, our results are based on hydrogel simulations, but it would be interesting to apply such analysis also to ultra-low-crosslinked microgels. In this respect, the microfluidic approach to microgels synthesis appears to be particularly promising, because it allows to prepare microgels of sizes of the order of $100\mu\text{m}$ [35, 36]. Furthermore, a specific method to calculate their elastic properties, known as capillary micromechanics, was already established, making these ideal model systems, already available in the literature, to test the present numerical predictions. Regarding hydrogels, it is worth recalling that the interest in their elastic properties has so far been mainly focused on their temperature dependence around the Volume Phase Transition, where critical behavior associated to the thermoresponsivity of the systems was observed and tentatively attributed to the Ising universality class [37–39]. The present work shifts the current paradigm to networks in good solvent, where the monomer affinity to the solvent does not change and the underlying interactions are always dominated by excluded volume. Indeed, in the present work it is a low enough connectivity that generates a non-trivial interplay with steric interactions under a small tension. To this aim, we remark that the pressures at which ν reaches its minimum at c^* is of the order of $P \sim 10^{-5}k_B T/\sigma^2$ (see Fig. 2(b) in SI), while the system volume V fluctuates around $\sim 10^6 - 10^7\sigma^3$ (see Methods for simulation units). This implies that the product PV is at worst 4 orders of magnitude smaller than the total energy scale of the system $\sim 20Nk_B T$ (see Fig. S5), where $N \approx 10^4$ is the total number of monomers in our simulations. This confirms that the phenomenology that we observe is another example of entropic phase transition [40, 41], as also evident in Figs. 3(f) and S6. The dominant role of connectivity and the different interactions with respect to a standard attractive system (e.g. a Lennard-Jones fluid) may then be the reason why the critical-like fluctuations of the present ultra-low-crosslinked hydrogels are not found to obey Ising universality class. Further numerical and theoretical work on this issue will be needed in the future. While the former should aim, in particular, to probe the critical fluctuations in a more extensive time and length window as well as to vary c in a more continuous fashion (e.g. by developing appropriate crosslinker insertion/deletion methods), the latter should be devoted to provide a new description of the mechanical instability, taking into account the connectivity, similarly to what discussed for the Volume Phase Transition [42]. Notwithstanding this, our results predict the existence of experimentally-realizable polymeric materials with highly tunable elastic properties that appear to be directly related to the occurrence of an unusual phase transition, opening up a new research direction in statistical and soft matter physics.

Methods We perform Molecular Dynamics simulations of polymer networks made of monomers interacting via the Kremer-Grest potential. Excluded volume for all particles are given by the Weeks-Chandler-Andersen potential: [43]

$$V_{WCA}(r) = \begin{cases} 4\epsilon \left[\left(\frac{\sigma}{r}\right)^{12} - \left(\frac{\sigma}{r}\right)^6 \right] + \epsilon & \text{if } r \leq 2^{1/6}\sigma \\ 0 & \text{if } r > 2^{1/6}\sigma \end{cases} \quad (1)$$

where σ is the particle diameter, which sets the unit of length, and ϵ controls the energy scale. Defining m as the mass of the particles, the unit time of our simulations is defined as $\tau = \sqrt{m\sigma^2/\epsilon}$. Chemical bonds between connected monomers are modeled by a FENE potential $V_{FENE}(r)$: [44]

$$V_{FENE}(r) = -\epsilon k_F R_0^2 \ln \left[1 - \left(\frac{r}{R_0\sigma} \right) \right] \quad \text{if } r < R_0\sigma \quad (2)$$

where $k_F = 15$ is the spring constant and $R_0 = 1.5$ is the maximum extension of the bond. We both consider ordered diamond-like and disordered topologies. In the former case, we prepare systems made up of 8 unitary cells, each containing 8 crosslinkers, that are placed on the lattice atom positions and are connected through chains of equal length [45, 46]. For each crosslinker concentration c , the network is composed of $N = 64/c$ monomers forming chains of equal length $l = (1 - c)/(2c)$. To produce disordered networks, we use the method recently developed in Ref. [24], which exploits the self-assembly of binary mixtures of patchy particles with valence $f = 2$ (monomers) and $f = 4$ (crosslinkers). We let the system equilibrate at low enough temperature ($T = 0.03$) through the oxDNA simulation package [47] until 99.9% of the bonds are formed by exploiting a recently devised swap algorithm [48]. Then, we select the largest cluster from which we remove dangling ends and replace patchy interactions with the bead-spring ones

(Eqns. 1 and 2). We obtain systems with final crosslinker concentrations $c \sim 1, 3, 5\%$ with deviation from the nominal values smaller than 5%. For $c \sim 1\%$ we consider three independent network realizations to assess the dependence of results on the specific topology.

For both ordered and disordered networks we perform NPT simulations using LAMMPS simulation package [49] with a Nosé - Hoover thermostat and barostat. We fix the temperature $T = 1.0\epsilon/k_B$, where k_B is the Boltzmann constant, and perform simulations at different (negative) pressures employing a timestep $\delta t = 0.003\tau$. We perform two kinds of simulations: (i) via equilibrium simulations in which the box is allowed to fluctuate anisotropically we calculate the bulk modulus K from volume fluctuations as $K = k_B T \frac{\langle V \rangle}{\langle V^2 \rangle - \langle V \rangle^2}$; (ii) via stress-strain simulations we simultaneously calculate Y and ν . In particular, we first apply a longitudinal extensional strain $\lambda_{\parallel} = (L_{\parallel} - L_{\parallel}^0)/L_{\parallel}^0$, where L_{\parallel}^0 and L_{\parallel} are the initial and final box lengths along the deformation axis, respectively. The range of deformation values encompasses $\lambda_{\parallel} \in [0, 0.3]$, at which the response is in the linear regime, and we use a fixed strain rate $\dot{\lambda} = 0.01\tau^{-1}$. The box is allowed to fluctuate transversally to the deformation in order to guarantee a constant average P . Then, once the system acquires the desired strain, the stress σ_{\parallel} along the deformation axis is calculated from the virial stress tensor and averaged over $10^6\tau$, yielding $Y = \sigma_{\parallel}/\lambda_{\parallel}$. The Poisson's ratio is instead extracted from transversal fluctuations through the relation $\nu = -\partial\lambda_{\perp}/\partial\lambda_{\parallel}$, where $\lambda_{\perp} \equiv (\lambda_2 + \lambda_3)/2$ and λ_2, λ_3 are the components of the strain orthogonal to the deformation axis. For each network and each state point, results for Y and ν are averaged over 20 independent deformations in which the same configuration is deformed with different initial velocities taken from the Maxwell-Boltzmann distribution. This procedure is repeated for each configuration by deforming the network over all three directions independently, in order to improve the statistics of the results. The bond length l_{bond} is calculated from the time averages of the particle separations, while the single chain entropy s_l is obtained within the Langevin approximation [25]. We define an order parameter M as the zero average and unitary variance version of the order parameter $\tilde{M} = \rho + se_{nb}$, where ρ is the density, s is a mixing parameter and e_{nb} is the energy of non-bonded particles only. Finally, we perform a histogram reweighting in pressure for the order parameter M minimizing the mean-square error with the Ising prediction [31]. More details on the Methods are reported in the Supplementary Information.

We thank F. Goio Castro, L. Rovigatti and F. Sciortino for useful discussions. We acknowledge support from the European Research Council (ERC Consolidator Grant 681597, MIMIC) and from Sapienza University of Rome through the SAPIExcellence program.

SUPPLEMENTARY MATERIALS

SI. ELASTIC MODULI AT ULTRA-LOW CROSSLINKING: COMPARISON WITH LINEAR ELASTICITY THEORY

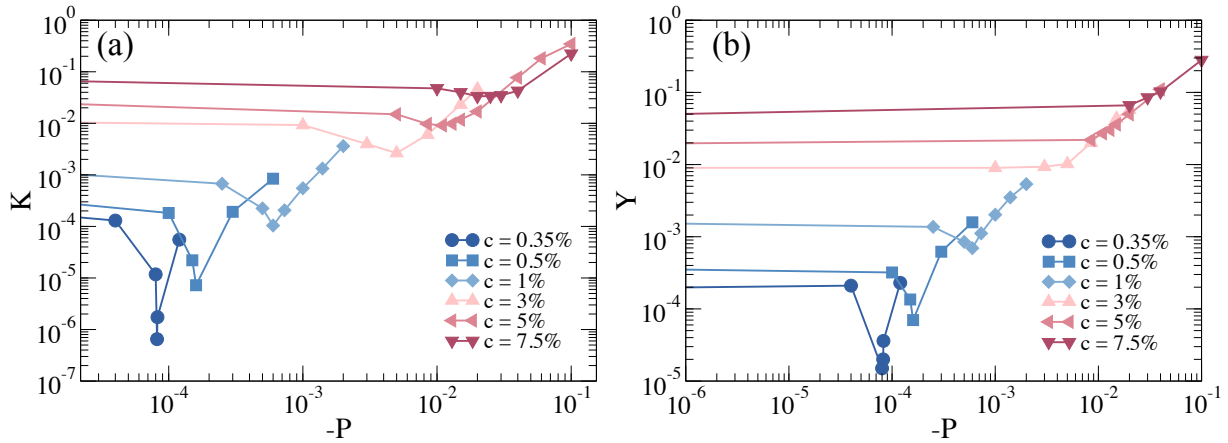


Figure S1. Bulk modulus K (a) and Young modulus (b) as a function of pressure for diamond networks with different crosslinker concentrations.

In Fig. S1 we report the bulk K and Young Y moduli as a function of pressure P for a diamond topology, with different crosslinker concentrations c . Both moduli at low c display a minimum, which becomes more pronounced upon further lowering c , at a characteristic (negative) value of P . Such values appear to be close but not exactly the same, within the current numerical resolution, as P_{min} , where the Poisson's ratio has a minimum, as discussed in the main text.

SII. DEPENDENCE ON NETWORK TOPOLOGY FOR DISORDERED REALIZATIONS

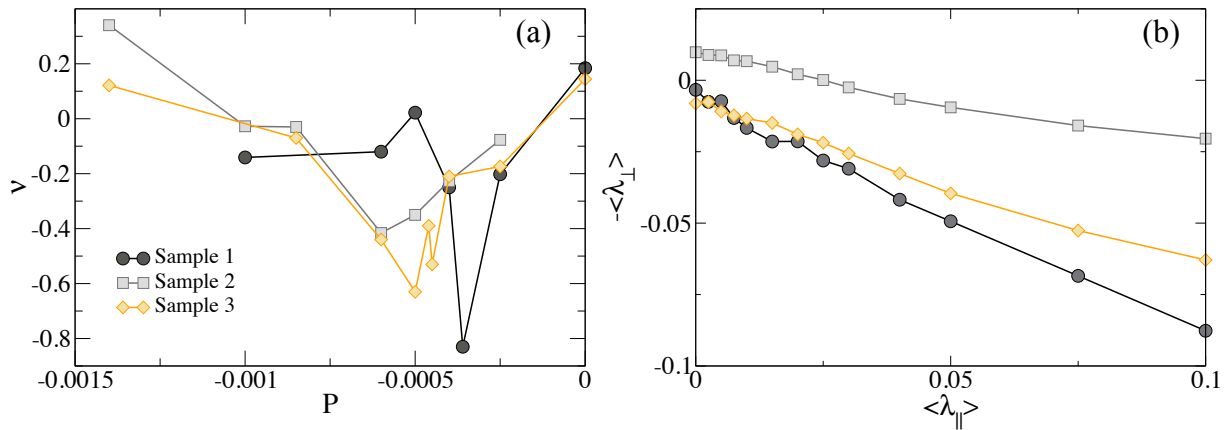


Figure S2. Stress-strain simulation results for the Dis - 1% network for three different topologies: (a) Poisson's ratio versus negative pressure; (b) negative transverse strain as a function of parallel strain for each topology at their respective $P_{min} = -3.6 \times 10^{-4}$, -5×10^{-4} , -6×10^{-4} for topology 1, 2 and 3, respectively.

In Fig. S2 we report results for the Poisson's ratio for different realizations of the Dis - 1% network, to show that we find consistent behaviour independent of the specific topology. In particular, Fig. S2(a) shows ν as a function of pressure for the three studied realizations, displaying a minimum in all cases, although taking place at different values of P_{min} . The transverse versus longitudinal strain for each P_{min} shows a similar behaviour for the different topologies, as reported in Fig. S2(b).

SIII. ELASTIC PROPERTIES FOR COMPRESSED AND EXPANDED (COEXISTING) STATES AT THE HYPER-AUXETIC POINT

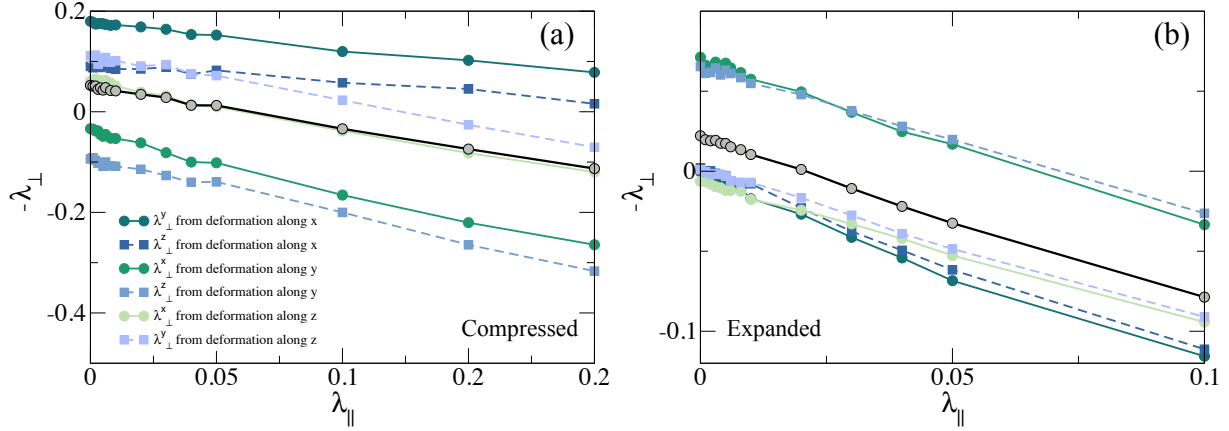


Figure S3. Results for the Diam - 0.35% network at $P_{min} = 8.19 \times 10^{-5}$: negative transverse strain obtained for the three axial directions as a function of parallel strain λ_{\parallel} both for the compressed (a) and the expanded (b) state.

Here we report the calculation of the elastic properties of the two coexisting compressed and elastic states for the Diam - 0.35% network at $P_{min} = 8.19 \times 10^{-5}$. We find that, even though the bulk modulus is much smaller in the expanded case ($K \sim 1.4 \times 10^{-6}$) as compared to the compressed ($K \sim 5.0 \times 10^{-6}$), the Poisson's ratio does not show a huge change, being $\nu \simeq -1$ for the expanded state and -0.84 for the compressed one. This can be seen from the calculated λ_{\perp} vs λ_{\parallel} for the compressed and expanded states, reported in Figs. S3(a),(b), respectively, for all examined deformation directions. These data suggest that a hyper-auxetic behaviour is found in both cases.

SIV. CRITICAL-LIKE BEHAVIOUR: DENSITY, ENERGY AND ENTROPY

Fig. S4 shows the onset of critical-like density fluctuations for the Diam - 0.35% system, as one gets close to the hyper-auxetic point for $P \sim P_{min}$.

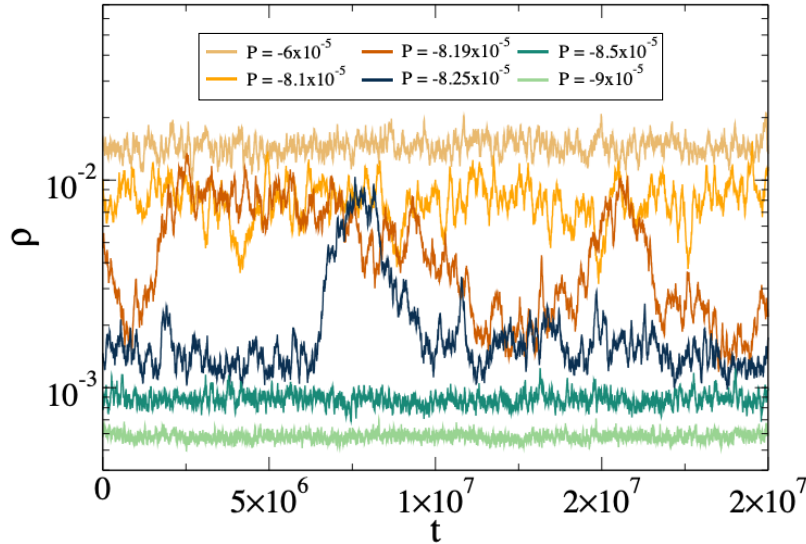


Figure S4. Density as a function of time for the Diam - 0.35% network at different negative pressures.

Fig. S5(a) reports the corresponding behavior in time of the total potential energy e_t . Interestingly, critical fluctuations are completely absent. We thus focus on the non-bonded potential energy e_{nb} , shown in Fig. S5(c), which

instead shows critical-like fluctuations. This correspondence is confirmed by the scatter plots, reported in Figs. S5(b) and (d), of total energy and non-bonded energy with density, respectively. Clearly, while the former appears to be not correlated with ρ , the second is. This analysis allows us to focus on e_{nb} as mixing variable in the order parameter M that controls the criticality of the transition, as discussed in the next section and in the main text.

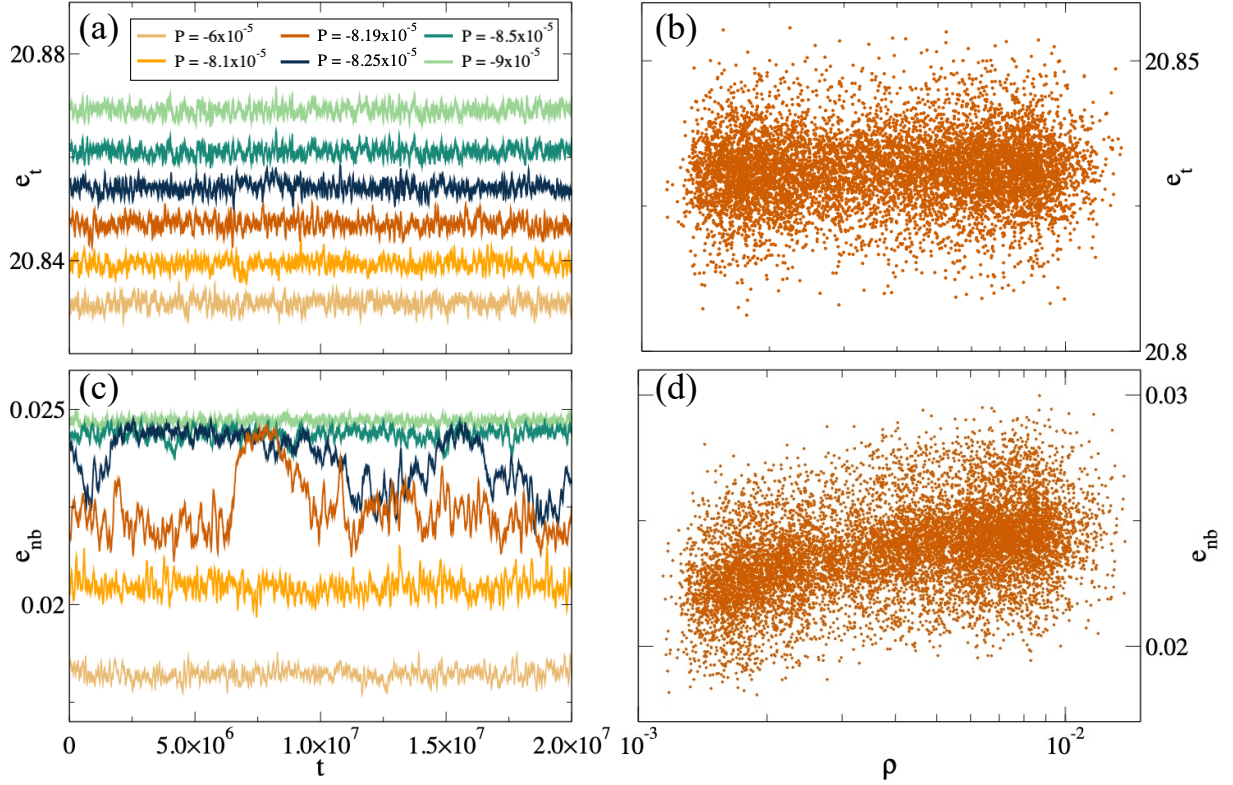


Figure S5. Energy as a function of time for the Diam - 0.35% network at different negative pressures: (a) total potential energy e_t and (c) non-bonded particle energy e_{nb} . Data for e_t are vertically translated by 0.05 with respect to each other to improve visualization; (b, d) scatter plots of the same quantities with respect to density ρ at $P_{min} = 8.19 \times 10^{-5}$.

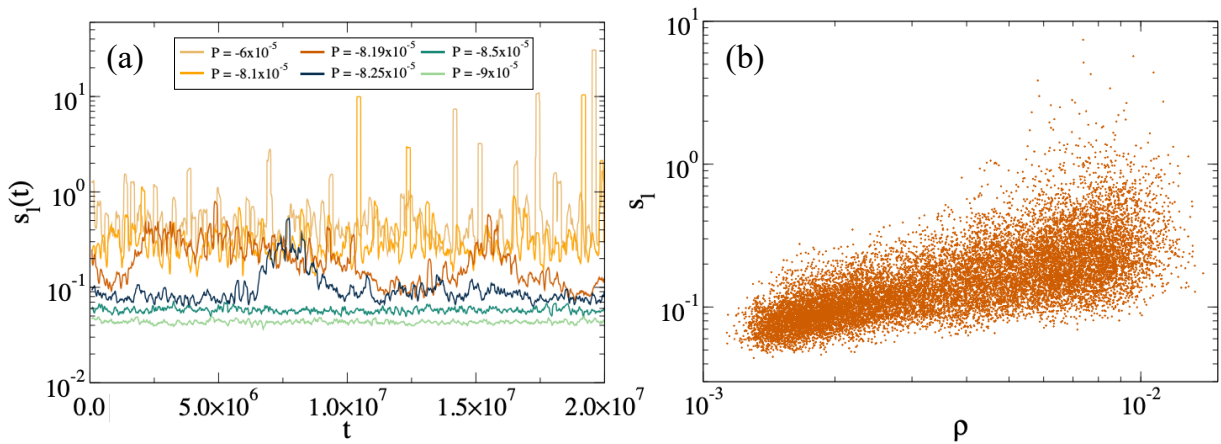


Figure S6. (a) Single chain entropy s_l as a function of time for the Diam - 0.35% at different negative pressures; (b) scatter plot of the same quantity with respect to density at $P_{min} = -8.19 \times 10^{-5}$.

As discussed in the main text, entropy plays an important role in the transition. In polymeric systems, the presence of crosslinkers and entanglements induces a constraint on the configurations that can be explored by the polymer chains. Typically, the chain end-to-end distance r can be used to describe chains fluctuations, whose probability

distribution has theoretically been approximated by a Gaussian distribution [30, 50]. In this way, the entropy of the network is computed as the sum of the contributions from every chain. While this approach was shown to be useful in dense systems, in dilute regimes it fails due to the presence of short chains whose r does not behave in a Gaussian way. Furthermore, by stretching the network, deviations from the gaussian behaviour will be significant [25]. To avoid these issues, here we calculate single chain entropy assuming that the end-to-end distance follows the Langevin approximation [30], which for a single chain is given by:

$$s_l^n(r) = k_B \left[-\frac{r}{b} \mathcal{L}^{-1}(r/nb) \right] \ln \left[\left(\frac{\mathcal{L}^{-1}(r/nb)}{\sinh \mathcal{L}^{-1}(r/nb)} \right)^{-n} \right] + A_n \quad (\text{S1})$$

where k_B is the Boltzmann constant, A_n is a temperature dependent parameter that can be set to zero, n is the number of monomers in the chains, b is the minimum value of the FENE interaction potential and $\mathcal{L}^{-1}(x)$ is the inverse Langevin function.

This approach has been shown to work relatively well in the case of phantom networks up to end-to-end distances approaching the contour length nb [25]. Thus, we define the average single chain entropy s_l as the average entropy of all the chains within the network which is reported in Fig. S6(a) for the same set of data reported in Fig S4. Interestingly, we observe critical-like jumps between a high entropy regime corresponding to high density and low entropy states corresponding to low density, which happen simultaneously with those occurring for density (Fig. S4) and non-bonded energy (Fig. S5(a)). This is confirmed by the scatter plot of entropy and density at P_{min} in Fig. S6(b).

SV. DENSITY DISTRIBUTIONS AND HISTOGRAM REWEIGHTING TECHNIQUE

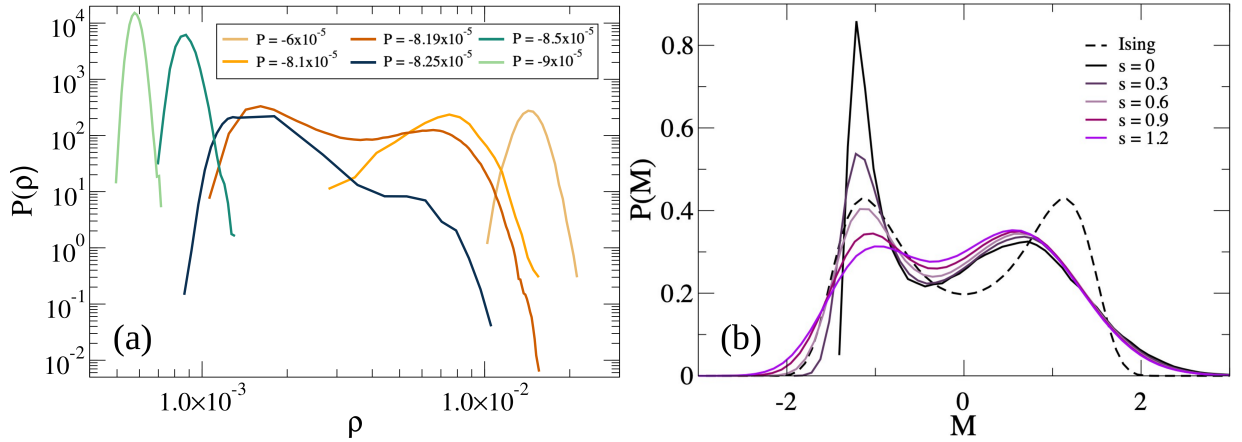


Figure S7. (a) Density distribution for different negative pressures for the Diam - 0.35% network; (b) distribution of the order parameter M at $P_{min} = -8.19 \times 10^{-5}$ for different values of the mixing parameter s . The dashed line is the reference Ising curve [31].

Close to the onset of the mechanical instability, the distribution of the density for different negative pressures for the Diam - 0.35% system is reported in Fig. S7(a). Here we employ the same set of data as in Fig. S4. We notice that, close to the transition, the system displays a bimodal distribution, that is highly asymmetric (note that data are reported in a log-log plot to improve visualization). In particular, we find the presence of a broad high-density peak and a narrow low-density one peak for low ones.

In order to connect to standard studies of phase transition, we further report in Fig. S7(b) the distribution of the order parameter $M = \rho - se_{nb}$, with zero average and unit variance, where we use the non-bonded rather than the total energy, for different values of the mixing parameter s for $P = P_{min}$. Fig. S7(b) shows that the presence of the mixing term is able to reduce the asymmetry of the original $P(\rho)$, but not completely. In particular, the height of the peaks becomes comparable for $s = 0.9$, but the difference in their variance remains at all s .

We thus resort to the histogram reweighting technique, which is a method that is particularly suitable to identify e.g. critical points of a thermodynamic phase transition, because it allows to extrapolate results to nearby state points, without having to perform simulations at all state points. However, in the present system, in order to get close to the critical point, we would need to vary in a continuous way both crosslinker concentration and pressure. While the latter is a thermodynamical variable that can be easily tuned, the former assumes discrete values in the ordered

system and cannot be finely controlled in the disordered system being the result of a self assembly procedure. We are thus forced to perform histogram reweighting only in pressure, while we need to perform numerous simulations at each c around P_{min} , pointing out the difficulty of the proper exploration of the critical conditions for the studied polymer networks. Our (single) histogram reweighting method, reported in Fig. 3 of the main text, relies then on the following expression:

$$P(V, e_{nb}; P') = \exp((P' - P)V)P(V, e_{nb}; P). \quad (S2)$$

SVI. SCALING PROPERTIES CLOSE TO THE TRANSITION

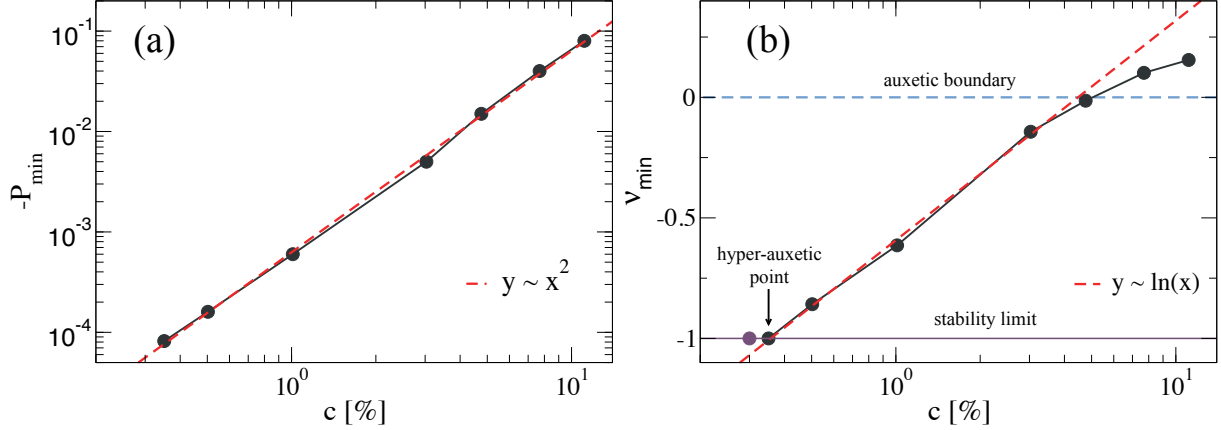


Figure S8. Minimum pressure P_{min} (a) and minimum Poisson's ratio ν_{min} (b) for diamond networks as a function of crosslinker concentration. Fits to the data are shown as dashed lines: in (a) a power law fit is used, while in (b) we employ a logarithmic function. The horizontal lines in (b) indicates $\nu = 0$ (dashed), below which auxetic behavior starts, and $\nu = -1$ (solid), that sets the limit of stability of the network. Note that for $c < c^*$ deviations from the logarithmic fit are observed, because the minimum Poisson's ratio always remains equal to -1.

In Fig S8 we report the behavior of P_{min} and ν_{min} as a function of crosslinker concentration for diamond networks. It is interesting that P_{min} closely follows a quadratic power-law behavior for $c \lesssim 1\%$, suggesting a critical behavior that would terminate at $c = 0$. Instead, ν_{min} follows a logarithmic behavior in c in the auxetic region, which ends at c^* , below which the minimum Poisson's ratio saturates at -1, the minimum value for a mechanically stable solid. For $c < c^*$ we indeed still detected $\nu_{min} = -1$, followed by a first-order transition between the two states upon further decreasing pressure.

-
- [1] Lakes, R. Foam structures with a negative poisson's ratio. *Science* **235**, 1038–1040 (1987).
 - [2] Evans, K. E. & Caddock, B. D. Microporous materials with negative poisson's ratios. ii. mechanisms and interpretation. *Journal of Physics D: Applied Physics* **22**, 1883–1887 (1989).
 - [3] Evans, K. E., Nkansah, M., Hutchinson, I. & Rogers, S. Molecular network design. *Nature* **353**, 124–124 (1991).
 - [4] Gatt, R. *et al.* Negative poisson's ratios in tendons: An unexpected mechanical response. *Acta Biomaterialia* **24**, 201–208 (2015).
 - [5] Hu, H. Auxetic textile materials - a review. *Journal of Textile Engineering & Fashion Technology* **1** (2017).
 - [6] Rysaeva, L. K., Baimova, J. A., Lisovenko, D. S., Gorodtsov, V. A. & Dmitriev, S. V. Elastic properties of fullerites and diamond-like phases. *physica status solidi (b)* **256**, 1800049 (2018).
 - [7] Greaves, G. N., Greer, A., Lakes, R. S. & Rouxel, T. Poisson's ratio and modern materials. *Nature materials* **10**, 823–837 (2011).
 - [8] Larsen, U., Signund, O. & Bouwsta, S. Design and fabrication of compliant micromechanisms and structures with negative poisson's ratio. *Journal of Microelectromechanical Systems* **6**, 99–106 (1997).
 - [9] Theocaris, P. S., Stavroulakis, G. E. & Panagiotopoulos, P. D. Negative poisson's ratios in composites with star-shaped inclusions: a numerical homogenization approach. *Archive of Applied Mechanics (Ingenieur Archiv)* **67**, 274–286 (1997).
 - [10] Hanifpour, M., Petersen, C. F., Alava, M. J. & Zapperi, S. Mechanics of disordered auxetic metamaterials. *The European Physical Journal B* **91** (2018).

- [11] Reid, D. R. *et al.* Auxetic metamaterials from disordered networks. *Proceedings of the National Academy of Sciences* **115**, E1384–E1390 (2018).
- [12] Dong, L., Stone, D. S. & Lakes, R. S. Softening of bulk modulus and negative poisson ratio in barium titanate ceramic near the curie point. *Philosophical Magazine Letters* **90**, 23–33 (2010).
- [13] Kou, L. *et al.* Auxetic and ferroelastic borophane: A novel 2d material with negative poisson’s ratio and switchable dirac transport channels. *Nano Letters* **16**, 7910–7914 (2016).
- [14] Landau, L. & Lifshitz, E. Theory of elasticity (volume 7 of a course of theoretical physics) pergamon press (1970).
- [15] Hirotsu, S. Softening of bulk modulus and negative poisson’s ratio near the volume phase transition of polymer gels. *The Journal of Chemical Physics* **94**, 3949–3957 (1991).
- [16] Li, C., Hu, Z. & Li, Y. Poisson’s ratio in polymer gels near the phase-transition point. *Physical Review E* **48**, 603–606 (1993).
- [17] Hirotsu, S. Static and time-dependent properties of polymer gels around the volume phase transition. *Phase Transitions* **47**, 183–240 (1994).
- [18] Wojciechowski, K. Two-dimensional isotropic system with a negative poisson ratio. *Physics Letters A* **137**, 60–64 (1989).
- [19] Boal, D. H., Seifert, U. & Shillcock, J. C. Negative poisson ratio in two-dimensional networks under tension. *Physical Review E* **48**, 4274–4283 (1993).
- [20] Bachman, H. *et al.* Ultrasoft, highly deformable microgels. *Soft Matter* **11**, 2018–2028 (2015).
- [21] Virtanen, O. L. J., Mourran, A., Pinard, P. T. & Richtering, W. Persulfate initiated ultra-low cross-linked poly(n-isopropylacrylamide) microgels possess an unusual inverted cross-linking structure. *Soft Matter* **12**, 3919–3928 (2016).
- [22] Scotti, A. *et al.* Deswelling of microgels in crowded suspensions depends on cross-link density and architecture. *Macromolecules* **52**, 3995–4007 (2019).
- [23] Scotti, A. *et al.* Exploring the colloid-to-polymer transition for ultra-low crosslinked microgels from three to two dimensions. *Nature Communications* **10** (2019).
- [24] Gnan, N., Rovigatti, L., Bergman, M. & Zaccarelli, E. In silico synthesis of microgel particles. *Macromolecules* **50**, 8777–8786 (2017).
- [25] Sorichetti, V. *et al.* The effect of chain polydispersity on the elasticity of disordered polymer networks. *Macromolecules* (2021). arXiv:2101.09814.
- [26] Xinchun, S. & Lakes, R. S. Stability of elastic material with negative stiffness and negative poisson’s ratio. *phys. stat. sol. (b)* **244**, 1008–1026 (2007).
- [27] Nicolaou, Z. G. & Motter, A. E. Mechanical metamaterials with negative compressibility transitions. *Nature Materials* **11**, 608–613 (2012).
- [28] Higgs, P. & Ball, R. Polydisperse polymer networks: elasticity, orientational properties, and small angle neutron scattering. *Journal de Physique* **49**, 1785–1811 (1988).
- [29] Grest, G. S. & Kremer, K. Statistical properties of random cross-linked rubbers. *Macromolecules* **23**, 4994–5000 (1990).
- [30] Pethrick, R. Polymer physics. edited by michael rubinstein and ralph h colby oxford university press, oxford, 2003. ISBN 019852059x. pp 440. *Polymer International* **53**, 1394–1395 (2004).
- [31] Wilding, N. B. & Bruce, A. D. Density fluctuations and field mixing in the critical fluid. *Journal of Physics: Condensed Matter* **4**, 3087–3108 (1992).
- [32] Debenedetti P. G., Z. G. H., Sciortino F. Second critical point in two realistic models of water. *Science* **369**, 289–292 (2020).
- [33] Gao, J. & Frisken, B. J. Cross-linker-Free N-isopropylacrylamide gel nanospheres. *Langmuir* **19**, 5212–5216 (2003).
- [34] Scotti, A. *et al.* Flow properties reveal the particle-to-polymer transition of ultra-low crosslinked microgels. *Soft matter* **16**, 668–678 (2020).
- [35] Seiffert, S. Impact of polymer network inhomogeneities on the volume phase transition of thermoresponsive microgels. *Macromolecular Rapid Communications* **33**, 1135–1142 (2012).
- [36] Voudouris, P., Florea, D., van der Schoot, P. & Wyss, H. M. Micromechanics of temperature sensitive microgels: dip in the poisson ratio near the LCST. *Soft Matter* **9**, 7158 (2013).
- [37] Li, Y. & Tanaka, T. Study of the universality class of the gel network system. *The Journal of Chemical Physics* **90**, 5161–5166 (1989).
- [38] Onuki, A. Theory of phase transition in polymer gels. In *Responsive Gels: Volume Transitions I*, 63–121 (Springer Berlin Heidelberg, 1993).
- [39] Habicht, A., Schmolke, W., Lange, F., Saalwächter, K. & Seiffert, S. The non-effect of polymer-network inhomogeneities in microgel volume phase transitions: Support for the mean-field perspective. *Macromolecular Chemistry and Physics* **215**, 1116–1133 (2014).
- [40] Frenkel, D. Entropy-driven phase transitions. *Physica A: Statistical Mechanics and its Applications* **263**, 26–38 (1999).
- [41] Sciortino, F. Entropy in self-assembly. *La Rivista del Nuovo Cimento* **42**, 511–548 (2019).
- [42] Dimitriyev, M. S., Chang, Y.-W., Goldbart, P. M. & Fernández-Nieves, A. Swelling thermodynamics and phase transitions of polymer gels. *Nano Futures* **3**, 042001 (2019).
- [43] Weeks, J. D., Chandler, D. & Andersen, H. C. Role of repulsive forces in determining the equilibrium structure of simple liquids. *The Journal of chemical physics* **54**, 5237–5247 (1971).
- [44] Kremer, K. & Grest, G. S. Dynamics of entangled linear polymer melts: A molecular-dynamics simulation. *The Journal of Chemical Physics* **92**, 5057–5086 (1990).
- [45] Claudio, G. C., Kremer, K. & Holm, C. Comparison of a hydrogel model to the poisson-boltzmann cell model. *The Journal of chemical physics* **131**, 094903 (2009).

- 381 [46] Jha, P. K., Zwanikken, J. W., Detchevery, F. A., De Pablo, J. J. & De La Cruz, M. O. Study of volume phase transitions
382 in polymeric nanogels by theoretically informed coarse-grained simulations. *Soft Matter* **7**, 5965–5975 (2011).
- 383 [47] Poppleton, E., Romero, R., Mallya, A., Rovigatti, L. & Šulc, P. Oxdna.org: a public webserver for coarse-grained
384 simulations of dna and rna nanostructures. *Nucleic Acids Research* (2021).
- 385 [48] Sciortino, F. Three-body potential for simulating bond swaps in molecular dynamics. *The European Physical Journal E*
386 **40** (2017).
- 387 [49] Plimpton, S. Fast parallel algorithms for short-range molecular dynamics. *Journal of computational physics* **117**, 1–19
388 (1995).
- 389 [50] Mark, J. E. *et al. Physical properties of polymers handbook*, vol. 1076 (Springer, 2007).